

Spectral Graph Reasoning Network for Hyperspectral Image Classification

Huiling Wang  *

Computing Sciences, Tampere University, Finland

Abstract. Convolutional neural networks (CNNs) have achieved remarkable performance in hyperspectral image (HSI) classification over the last few years. Despite the progress that has been made, rich and informative spectral information of HSI has been largely underutilized by existing methods which employ convolutional kernels with limited size of receptive field in the spectral domain. To address this issue, we propose a spectral graph reasoning network (SGR) learning framework comprising two crucial modules: 1) a spectral decoupling module which unpacks and casts multiple spectral embeddings into a unified graph whose node corresponds to an individual spectral feature channel in the embedding space; the graph performs interpretable reasoning to aggregate and align spectral information to guide learning spectral-specific graph embeddings at multiple contextual levels 2) a spectral ensembling module explores the interactions and interdependencies across graph embedding hierarchy via a novel recurrent graph propagation mechanism. Experiments on two HSI datasets demonstrate that the proposed architecture can significantly improve the classification accuracy compared with the existing methods with a sizable margin.

1 Introduction

Hyperspectral image comprises hundreds of continuous spectral bands throughout the electromagnetic spectrum with high spectral resolution, which facilitates the precise differentiation of chemical properties of scene materials remotely. Consequently hyperspectral images have been considered as a crucial data source in various fields, such as environmental monitoring, mining, agriculture, and land-cover mapping.

HSI classification involves assigning a categorical class label to each individual pixel location given the corresponding spectral feature. Various classification approaches have been proposed to address the hyperspectral image classification problem. Early approaches largely adopted traditional machine learning methods which were trained on hand-crafted features from HSI data to empirically encode the spectral information, *e.g.* SVM [13], KNN [18], dictionary learning [2], graphical model [21], extreme learning machine [16] and among others. Other methods [29,28] also exploited both spectral and spatial information since utilizing only the spectral information regardless of the spatial correlation is difficult in accurately classifying different land-cover categories.

* huiling.wang@tuni.fi

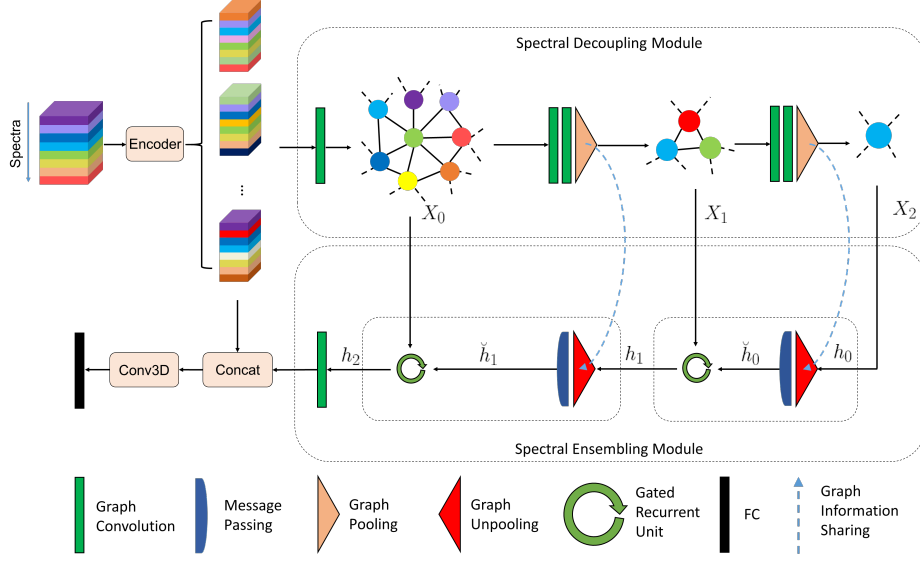


Fig. 1: Illustration of our proposed network architecture.

With the advent of new remote sensing instruments and increased temporal resolutions, the deluge of high dimensional HSI data is posing new challenges on the limited discriminative power of the empirically designed features and the traditional classification methods. Deep learning based HSI classification methods have been proposed inspired by its success in visual recognition of natural images. Those methods benefit from the strong representation capability and end-to-end learning. Chen *et al.* [4] developed the first deep neural networks (DNN) method which utilized stacked autoencoders to learn high-level features. Mou *et al.* [19] introduced a Recurrent Neural Network (RNN) based architecture. More powerful end-to-end Convolutional Neural Network (CNN) based architectures [3,8,11] have been proposed recently. Lee *et al.* [15] explored local contextual interactions by jointly exploiting local spatio-spectral relationships of neighboring pixels. Residual learning [9] was introduced by Song *et al.* [22] to build very deep network for extracting more discriminative feature representations for HSI classification. Li *et al.* [17] introduced a 3D-CNN architecture which was improved by He *et al.* [10] to jointly learn Multi-scale 2D spatial feature and 1D spectral feature from HSI data. Graph convolutional network (GCN) based approaches [20,26] have also been proposed which operated on graphs constructed in the *spatial* domain, aggregating and transforming feature information from the neighbors of every graph node given their relevance.

Despite of the significant improvements by the DNN based methods, they suffer from a number of inherent pitfalls. Specifically, all existing methods utilize convolutional kernels with limited size of receptive field to encode the very high dimensional and informative spectral domain. As a consequence, output constituting a certain new spectral channel is derived from only a fraction of all spectral channels which blocks information flow between distant spectra and fails

to capture longer term contextual information. Furthermore, spectral domain normally contains abundant yet noisy information which can lead to spurious classifications due to this weakened representation based on local contexts.

In this paper, we propose a novel spectral graph reasoning network (SGR) to explicitly address the above issues. Specifically, we firstly unpack and cast multiple spectral embeddings into a unified graph with each node corresponding to an individual spectral embedding channel via a novel spectral decoupling module. Graph reasoning facilitates the interactions between spectra which in turn boosts the representational capacity of the network by discriminating the significance of different spectral bands. A spectral-specific graph embedding hierarchy is generated through the spectral decoupling module which encodes a hierarchical representation of the spectral information. Each level of the hierarchy carries different degrees of discriminative power for HSI classification. To the best of our knowledge, this is the first method to model and interpret HSI data using graph neural network in the spectral domain.

We further introduce a spectral ensembling module that correlates the multi-contextual spectral-specific graph embeddings across the spectral hierarchy. This is achieved through a novel recurrent graph propagation mechanism which learns to map from a sequence of input graphs with varying size, each representing a state of transformed spectra with its intrinsic structure, to an ensembled spectral representation containing the key discriminative features from each contextual level to improve the classification accuracy.

2 Method

We propose a novel end-to-end spectral-specific graph representation learning framework for HSI classification, which comprises two core modules *i.e.* spectral decoupling module and spectral ensembling module, as illustrated in Fig. 1.

2.1 Graph Construction

We define a graph structure for mining correlations and constraints among spectral embedding channels. Specifically, we define an undirected graph $\mathcal{G} = (\mathcal{V}, \mathcal{E}, \mathcal{A})$. Given the feature map $X \in \mathbb{R}^{N \times H \times W}$ produced by the encoder network from an input HSI data volume centered at each pixel location, we seek to construct graph node set $\mathcal{V} = \{v_i\}_{i=1}^N$ and each node $v_i \in \mathcal{V}$ corresponds to a spectral feature from the embedding and the associated feature vector with $C = H \times W$ dimensions indicates $x_i \in \mathbb{R}^C$. The set of edges $\mathcal{E} = \{e_{ij}\}$ indicate the connection between nodes, and $\mathbf{A} = (e_{ij})_{N \times N}$ is the adjacency matrix, with $a_{i,j} = 0$ if $(i, j) \notin \mathcal{E}$, and $a_{i,j} = 1$ if $(i, j) \in \mathcal{E}$. We adopt K-Nearest Neighbor Graph (KNN-Graph) construction [27,23,24,25] in which two vertices v_i and v_j are connected by an edge, if the distance between v_i and v_j is among the k-th smallest distances measured by cosine distance. The normalized graph Laplacian [6] is computed as $L = I_N - D^{-\frac{1}{2}}AD^{-\frac{1}{2}}$, where $D^{ii} = \sum_j A^{ij}$.

The spectral convolutions on graphs [7] can be formulated as the multiplication of input $x \in \mathbb{R}^n$ with operator g_θ in Fourier domain,

$$y = g_\theta(L) * x = U g_\theta(\Lambda) U^T x \quad (1)$$

where graph Fourier basis U is the matrix of the eigenvectors of the normalized graph Laplacian L such that $L = U\theta(\Lambda)U^T$ with Λ being its corresponding eigenvalues, and $U^T x$ represents the graph Fourier transform of x . To reduce the computational complexity, Kipf and Welling [12] stacked multiple localized graph convolutional layers with the first-order approximation of graph Laplacian,

$$Y = \tilde{D}^{-\frac{1}{2}} \tilde{A} \tilde{D}^{-\frac{1}{2}} XW \quad (2)$$

where $W \in \mathbb{R}^{M \times F}$ is the matrix of filter parameters, \tilde{A} and \tilde{D} are the normalized versions with $\tilde{A} = A + I_N$ and $\tilde{D}^{ii} = \sum_j \tilde{A}^{ij}$.

2.2 Spectral Decoupling

The spectral decoupling module aims to learn spectral-specific feature representation by reasoning within spectral embedding at multiple scales. Necessitated by the excessive information of the broad and noisy spectral domain, this module explores the long-range contextual dependencies in the original feature space to form multiple lower dimensional intermediate representations in order to capture the essence of the spectral information.

We adopt a graph pyramid of spectral features - at each scale of the graph pyramid, graph convolution (GCN) is applied to capture the interdependence of graph via message passing between the nodes of graphs, *i.e.* spectral features, as illustrated in Fig. 1. Assuming that filters in later layers of an encoder are responsive to various materials that make up the scanned scene, the proposed band GCN captures correlations and occurrences between more abstract characteristics in the scene like constituent materials. Graph pooling is applied to reduce the resolution of spectral features, whose result forms the input of the following graph convolution layer.

Graph pooling aims to enable down-sampling on graph data while preserving as much information as possible from the original graph. To this end, we employ a single neuron linear layer parameterized by W_θ , followed by a sigmoid function and top- k pooling. This is implemented as multiplying the input at l th layer $X^l \in \mathbb{R}^{N \times C}$ with $W_\theta^l \in \mathbb{R}^C$ followed by sigmoid operation, whose result is an 1D vector $\mathbf{s} \in \mathbb{R}^N$ measuring how much information of nodes can be retained when projected onto the direction W_θ^l . Graph coarsening can thus be done by selecting nodes with the largest scalar projection values on W_θ^l to form a new graph. The location of selected nodes in the original graph is recorded for graph unpooling operation. The feature of the selected nodes is adjusted by its projection values as $X^{l+1} = X^l \odot \mathbf{s}$ where \odot is the Hadamard product. Intuitively the selected nodes represent the “cluster centers” of spectral features and the edges measure the similarity between these clusters.

2.3 Spectral Ensembling

Once obtaining a pyramid of graph embeddings after graph pooling, *i.e.* $\mathcal{X} = \{X_1, X_2, \dots, X_L\}$, with each level of the hierarchy encoding the key spectral-specific feature at a certain scale, we explore their interactions across the hierarchy via a novel recurrent spectral ensembling module. There are mainly two

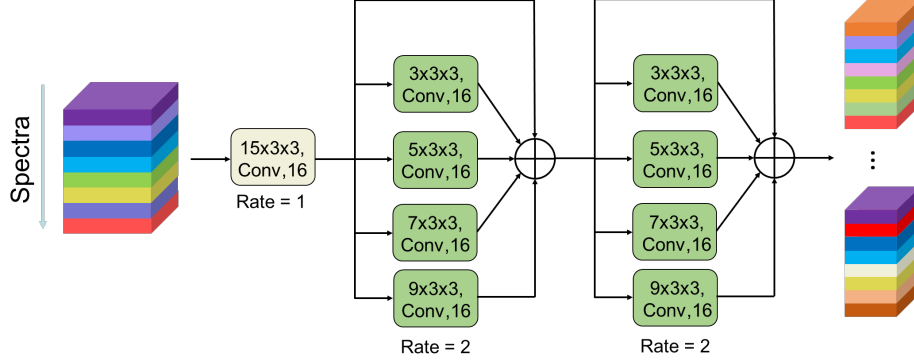


Fig. 2: Illustration of the encoder network.

challenges in ensembling a sequence of multi-level graph embeddings. Firstly, interaction between graphs of different number of nodes is not as straightforward as grid-like data *e.g.* images and texts due to the lack of spatial locality and order information. Note, the number of nodes in the graph corresponds to the cardinality of spectral embeddings. Secondly, recall that each of the previous graph pooling layer selected some important nodes to form a new graph for high-level feature encoding, the nodes in the new graph might become isolated due to the related edges have been removed while removing nodes.

In order to address the above issues, we propose a recurrent message passing ensembling mechanism. Specifically, for every two neighboring graph embeddings, the smaller but higher level graph is firstly unpooled to match the size of the bigger yet lower level graph. Then two graphs are interacting in a way that higher level graph is used as the hidden state encoding historical information, transferring its graph embedding and node interdependency to guide the message passing within the lower level graph. Fig. 1 illustrates the unrolled recurrent spectral ensembling where all the intermediate graph representations are processed as a sequence of input instances in the recurrent unit with shared weights.

Formally, indicating $\mathbf{h}_0 = X_L$, the graph unpooling layer l is defined as

$$\check{\mathbf{h}}_l = \text{MessagePassing}(f(0_{N \times C}, \mathbf{h}_l, \mathcal{I}), \mathcal{G}_{L-l}) \quad (3)$$

where \mathcal{I} represents the set of indices of selected nodes in the corresponding graph pooling layer $L - l$ which reduced the number of graph nodes from N to k (due to top- k pooling), $\mathbf{h}_l \in \mathbb{R}^{k \times C}$ is the feature map of current graph, $0_{N \times C}$ is the empty feature matrix for the new graph, $f(\cdot)$ indicates the mapping operation distributing row vectors of \mathbf{h}_l into $0_{N \times C}$ according to the corresponding indices in \mathcal{I} , \mathcal{G}_{L-l} indicates the graph definition before graph pooling layer $L - l$ which consists of affinity matrix and edge weights, and MessagePassing defines the message passing process [12] as

$$\check{\mathbf{h}}_l^i = \sum_{j \in \mathcal{N}(i) \cup \{i\}} \Theta \cdot \mathbf{h}_l^j, \quad (4)$$

Class No.	Class Name	Training	Testing
1	Asphalt	50	6581
2	Meadows	50	18599
3	Gravel	50	2049
4	Trees	50	3014
5	Painted metal sheets	50	1295
6	Bare Soil	50	4979
7	Bitumen	50	1280
8	Self-Blocking Bricks	50	3632
9	Shadows	50	897
Total		450	42776

Table 1: Sample size for the University of Pavia dataset.

where neighboring node features are first transformed by the weight matrix Θ passed via \mathcal{G}_{L-l} . The potential isolation of upsampled nodes in the new graph due to the removed related edges is properly compensated by the message passing based on the original graph interdependency information.

Then the framework updates the hidden state based on spectral feature X_{L-l} and hidden state \mathbf{h}_{l-1} from previous step via a gated mechanism similar to Gated Recurrent Unit (GRU) [5] as

$$\begin{aligned}
\mathbf{z}_l &= \sigma \left(\mathbf{W}_z X_{L-l} + \mathbf{U}_z \check{\mathbf{h}}_{l-1} \right), \\
\mathbf{r}_l &= \sigma \left(\mathbf{W}_r X_{L-l} + \mathbf{U}_r \check{\mathbf{h}}_{l-1} \right), \\
\tilde{\mathbf{h}}_l &= \tanh \left(\mathbf{W}_o X_{L-l} + \mathbf{U}_o (\mathbf{r}_l \odot \check{\mathbf{h}}_{l-1}) \right), \\
\mathbf{h}_l &= (1 - \mathbf{z}_l) \odot \check{\mathbf{h}}_{l-1} + \mathbf{z}_l \odot \tilde{\mathbf{h}}_l
\end{aligned} \tag{5}$$

where $\sigma(\cdot)$ is the logistic sigmoid function, $\tanh(\cdot)$ is the hyperbolic tangent function, and \odot is the Hadamard product. Interactions between all levels in the graph embedding hierarchy are enabled by encoding higher level contextual spectral information in the hidden states. The process is repeated L times according to the levels of hierarchy, and the final hidden state \mathbf{h}_L goes through another GCN layer before being concatenated with the feature map from the encoder network for predicting the category label of the input HSI volume with a fully connected layer.

2.4 Encoder Network

We adopt a multi-path dilated 3D convolutional residual network to encode the original HSI data as illustrated in Fig. 2. Specifically, the encoder starts with a 3D convolutional layer with kernel size $15 \times 3 \times 3$ corresponding to the spectral dimension and two spatial dimensions respectively, which is followed by two multi-path ($3 \times 3 \times 3$, $5 \times 3 \times 3$, $7 \times 3 \times 3$ and $9 \times 3 \times 3$ kernels respectively) dilated (rate=2) convolutional residual modules with identity shortcuts. Note that our proposed framework is agnostic to the utilized encoder network.

Class No.	Class Name	Training	Testing
1	Alfalfa	40	6
2	Corn-notill	100	1328
3	Corn-mintill	100	730
4	Corn	100	137
5	Grass-pasture	100	383
6	Grass-trees	100	630
7	Grass-pasture-mowed	20	8
8	Hay-windrowed	100	378
9	Oats	15	5
10	Soybean-notill	100	872
11	Soybean-mintill	100	2355
12	Soybean-clean	100	493
13	Wheat	100	105
14	Woods	100	1165
15	Buildings-Grass-Trees-Drives	100	286
16	Stone-Steel-Towers	80	13
Total		1355	8894

Table 2: Sample size for the Indian Pines dataset

3 Experimental Results

We evaluate our method on two publicly available hyperspectral image datasets with four metrics including per-class accuracy, overall accuracy (OA), average accuracy (AA), and Kappa coefficient. The network architecture of the proposed method SGR is identical for both datasets. Specifically, we use an architecture of $L=2$ and the input HSI is sampled on 7×7 image patches in the spatial domain. We adopt stochastic gradient descent with momentum set to 0.9, weight decay of 0.0005, and with a batch size of 30. We initialize an equal learning rate for all trainable layers to 0.05, which is manually decreased by a factor of 10 when the validation error plateaus. The number of training epochs is set to 500. All the reported accuracies are calculated based on the average of five training sessions to obtain stable results.

3.1 Datasets

The University of Pavia dataset was captured with the ROSIS sensor in 2001 which consists of 610×340 pixels with a spatial resolution of $1.3 \text{ m} \times 1.3 \text{ m}$ and has 103 spectral channels in the wavelength range from $0.43 \mu\text{m}$ to $0.86 \mu\text{m}$ after removing noisy bands. This dataset includes 9 land-cover classes and the false color image and ground-truth map are shown in Fig. 3.

The Indian Pines dataset was captured with Airborne Visible/Infrared Imaging Spectrometer sensor comprising 145×145 pixels with a spatial resolution of $20 \text{ m} \times 20 \text{ m}$ and 220 spectral channels covering the range from $0.4 \mu\text{m}$ to $2.5 \mu\text{m}$. This dataset includes 16 land-cover classes and the false color image and ground-truth map are shown in Fig. 4.

Table 1 and Table 2 provide information about all the classes of both datasets with their corresponding training and test samples respectively. During training,

Class No.	FCN [14]	MS 3D-CNN [10]	SS 3D-CNN [17]	3D-CNN [8]	SGR
1	61.98	92.47	91.98	91.86	95.91
2	72.16	94.22	93.88	90.55	98.27
3	12.90	86.38	81.46	85.89	88.47
4	39.52	92.63	94.98	93.65	99.83
5	99.46	98.57	100.00	98.59	99.91
6	41.78	80.45	74.34	70.49	84.75
7	50.49	83.60	84.94	84.66	86.42
8	67.99	90.30	86.92	88.58	91.43
9	97.55	97.43	99.94	98.82	98.24
OA	61.21	91.35	90.30	88.14	94.37
AA	60.42	90.67	89.82	89.23	93.69
Kappa	48.44	88.56	87.15	84.46	91.26

Table 3: Per-class accuracy, OA, AA (%), and Kappa coefficient achieved by different methods on the University of Pavia dataset.

90% of the training samples are used to learn the network parameters and 10% are used as validation set for tuning the hyperparameters.

3.2 Classification Results

The University of Pavia Dataset The quantitative results obtained by different approaches on the University of Pavia dataset are reported in Table 3. Our method outperforms the compared methods on 7 out of 9 categories and achieves the best overall results, *i.e.* OA, AA and Kappa. Generally, all other networks significantly outperform FCN [14]. One possible reason could be that FCN heavily squeezed the spectral dimension and utilized small 2D convolutional kernels in the spatial domain. 3D-CNN [8] adopted more 3D convolutional layers to perform simultaneous spatial-spectral convolution. Compared with [14], [8] used a large number of 3D filters per layer to improve the feature representation over the very high dimensional spectral domain which increases the accuracy by $\sim 2\%$. [10] addresses the limitations of single scale 3D CNN architectures by introducing a multi-scale 3D CNN architecture, which improves the accuracy by $\sim 1\%$ compared to [8]. Nevertheless, none of the existing methods has explicitly performed reasoning among the spectral embedding channels in a global manner, but rather modeling the local context by convolutional kernels with limited size of receptive field. Our method bridges this gap by casting spectral embeddings into a unified graph whose node corresponds to an individual spectral feature in the embedding space and thus the interaction between graph nodes guides learning spectral-specific graph representations. Quantitative results shows that our method outperforms the best competing method [10] with a significant margin of 3.02%.

Fig. 3 shows a visual comparison of our proposed SGR and the best competing method [10] on the University of Pavia dataset. The observation reveals that [10] suffers more mis-classifications than SGR in large semantically coherent regions, due to its weaker representation capability of encoding the discriminative spectral features with the presence of noise. The qualitative result that our SGR produces more accurate and coherent predictions.

Class No.	FCN [14]	SS 3D-CNN [17]	MS 3D-CNN [10]	3D-CNN [8]	SGR
1	6.7	80.00	100.00	30.77	99.56
2	64.81	76.41	77.52	70.90	79.32
3	74.67	78.06	79.36	76.12	80.47
4	59.21	76.65	80.85	77.46	83.72
5	92.19	92.16	96.43	90.96	97.62
6	97.66	99.13	99.84	96.86	99.92
7	47.56	40.00	100.00	48.48	100.00
8	97.04	99.87	100.00	97.70	100.0
9	16.95	58.82	100.00	71.43	100.00
10	78.71	76.75	79.84	70.07	81.55
11	76.59	80.09	82.50	77.83	85.26
12	65.23	78.03	76.56	68.31	80.97
13	98.51	97.65	99.53	95.57	99.92
14	94.88	94.64	97.34	96.12	98.75
15	70.75	73.96	85.53	71.70	85.97
16	49.33	89.66	100.00	78.79	100.00
OA	79.20	83.37	85.79	80.35	87.83
AA	68.17	80.74	90.96	76.19	92.06
Kappa	75.89	80.89	83.58	77.19	85.42

Table 4: Per-class accuracy, OA, AA (%), and Kappa coefficient achieved by different methods on the Indian Pines dataset

The Indian Pines Dataset Table 4 gives the quantitative results on the Indian Pines dataset, which shows that the proposed method obtains the best overall accuracy of 87.83%. Similar observations with the University of Pavia dataset can be found that all 3D CNN architectures outperform FCN [14] which adopts small 2D convolutional kernels as majority components. 3D CNN architectures generally explore the spatial-spectral contexts simultaneously and achieves better accuracy. Nevertheless, our proposed method has the advantage over the compared methods by exploring inter-spectral relations and learning a graph embedding hierarchy representation with each level emphasizing on specific spectral features exhibiting discriminative power toward the classification. Fig. 4 shows a visual comparison of our proposed SGR and the second best method [10], which confirms that our SGR produces more accurate and coherent predictions.

3.3 Ablation Study

We conduct ablation study on the University of Pavia dataset to quantitatively verify the effectiveness of the proposed architecture. The first baseline is applying a predicting layer (Conv3D-FC-Softmax) on top of the encoder network, *i.e.* Baseline-1. We also investigate spectral decoupling module with two different depth 1 and 3, dubbed as Baseline-2 and Baseline-3 respectively. To verify the contribution from spectral ensembling, we replace it with a naive graph upsampling and embedding summation operation, *i.e.* Baseline-4.

As shown in Table 5, a significant accuracy gain of 6.13% is achieved by our proposed spectral graph reasoning network, by comparing Baseline-1 and SGR.

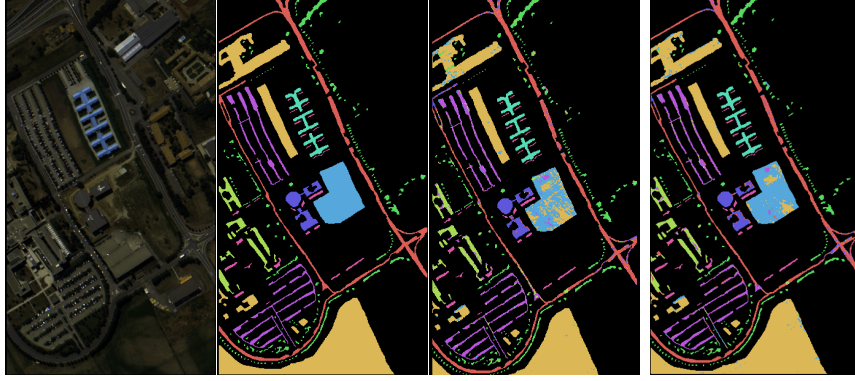


Fig. 3: The university of Pavia dataset: (a) False color image (b) Groundtruth map (c) Prediction of SSLSTMs [30] (d) Prediction of the proposed SPGAT

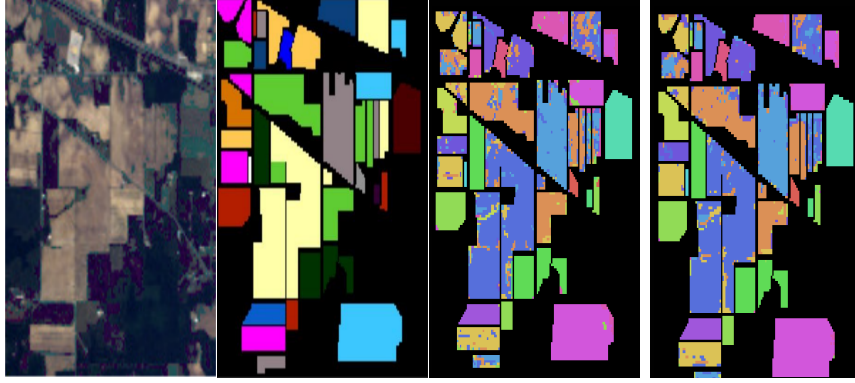


Fig. 4: Indian Pines dataset: (a) False color image (b) Groundtruth map (c) Prediction of LBMSELM [1] (d) Prediction of the proposed SPGAT

	Baseline-1	Baseline-2	Baseline-3	Baseline-4	SGR
OA	88.24	91.87	94.21	92.54	94.37

Table 5: OA achieved by different baselines on the University of Pavia dataset.

Adding one level of spectral coupling module improves the accuracy from 88.24% to 91.87%, which confirms its effectiveness. However, adding three levels slightly decreases the accuracy, *i.e.* a loss of 0.16% compared with SGR which has two levels. The possible reason is using the limited training samples for learning a more complex architecture. Furthermore, introducing the spectral ensembling module boosts the performance by 1.83%.

4 Conclusions

In this paper, we proposed a novel spectral graph reasoning network for hyperspectral image classification which has significantly advanced the state-of-the-art. At the core of our network architecture lies a new spectral feature reasoning and ensembling paradigm. We demonstrated that applying interpretable graph reasoning in the spectral feature domain enables learning a spectral-specific graph embedding which in turn improves the discriminative capability. We further proposed a spectral ensembling module that explores the interactions and interdependencies across the graph embedding hierarchy via a novel recurrent message propagation mechanism.

References

1. Cao, F., Yang, Z., Ren, J., Chen, W., Han, G., Shen, Y.: Local block multilayer sparse extreme learning machine for effective feature extraction and classification of hyperspectral images. *IEEE Trans. Geoscience and Remote Sensing* 57(8), 5580–5594 (2019)
2. Chen, Y., Nasrabadi, N.M., Tran, T.D.: Hyperspectral image classification using dictionary-based sparse representation. *IEEE transactions on geoscience and remote sensing* 49(10), 3973–3985 (2011)
3. Chen, Y., Jiang, H., Li, C., Jia, X., Ghamisi, P.: Deep feature extraction and classification of hyperspectral images based on convolutional neural networks. *IEEE Transactions on Geoscience and Remote Sensing* 54(10), 6232–6251 (2016)
4. Chen, Y., Lin, Z., Zhao, X., Wang, G., Gu, Y.: Deep learning-based classification of hyperspectral data. *IEEE Journal of Selected topics in applied earth observations and remote sensing* 7(6), 2094–2107 (2014)
5. Cho, K., van Merriënboer, B., Gülçehre, Ç., Bahdanau, D., Bougares, F., Schwenk, H., Bengio, Y.: Learning phrase representations using RNN encoder-decoder for statistical machine translation. In: *EMNLP*. pp. 1724–1734. *ACL* (2014)
6. Chung, F.R., Graham, F.C.: *Spectral graph theory*. No. 92, American Mathematical Soc. (1997)
7. Defferrard, M., Bresson, X., Vandergheynst, P.: Convolutional neural networks on graphs with fast localized spectral filtering. In: *Advances in neural information processing systems*. pp. 3844–3852 (2016)
8. Hamida, A.B., Benoit, A., Lambert, P., Amar, C.B.: 3-d deep learning approach for remote sensing image classification. *IEEE Transactions on geoscience and remote sensing* 56(8), 4420–4434 (2018)
9. He, K., Zhang, X., Ren, S., Sun, J.: Deep residual learning for image recognition. In: *Proceedings of the IEEE Conference on Computer Vision and Pattern Recognition*. pp. 770–778 (2016)
10. He, M., Li, B., Chen, H.: Multi-scale 3d deep convolutional neural network for hyperspectral image classification. In: *2017 IEEE International Conference on Image Processing (ICIP)*. pp. 3904–3908. *IEEE* (2017)
11. Hu, X., Wang, X., Zhong, Y., Zhao, J., Luo, C., Wei, L.: Spnet: A spectral patching network for end-to-end hyperspectral image classification. In: *IGARSS 2019-2019 IEEE International Geoscience and Remote Sensing Symposium*. pp. 963–966. *IEEE* (2019)
12. Kipf, T.N., Welling, M.: Semi-supervised classification with graph convolutional networks. In: *Proceedings of International Conference on Learning Representations* (2017)

13. Kuo, B.C., Huang, C.S., Hung, C.C., Liu, Y.L., Chen, I.L.: Spatial information based support vector machine for hyperspectral image classification. In: 2010 IEEE International Geoscience and Remote Sensing Symposium. pp. 832–835. IEEE (2010)
14. Lee, H., Kwon, H.: Contextual deep cnn based hyperspectral classification. In: 2016 IEEE International Geoscience and Remote Sensing Symposium (IGARSS). pp. 3322–3325. IEEE (2016)
15. Lee, H., Kwon, H.: Going deeper with contextual cnn for hyperspectral image classification. *IEEE Transactions on Image Processing* 26(10), 4843–4855 (2017)
16. Li, W., Chen, C., Su, H., Du, Q.: Local binary patterns and extreme learning machine for hyperspectral imagery classification. *IEEE Transactions on Geoscience and Remote Sensing* 53(7), 3681–3693 (2015)
17. Li, Y., Zhang, H., Shen, Q.: Spectral–spatial classification of hyperspectral imagery with 3d convolutional neural network. *Remote Sensing* 9(1), 67 (2017)
18. Ma, L., Crawford, M.M., Tian, J.: Local manifold learning-based k -nearest-neighbor for hyperspectral image classification. *IEEE Transactions on Geoscience and Remote Sensing* 48(11), 4099–4109 (2010)
19. Mou, L., Ghamisi, P., Zhu, X.X.: Deep recurrent neural networks for hyperspectral image classification. *IEEE Transactions on Geoscience and Remote Sensing* 55(7), 3639–3655 (2017)
20. Qin, A., Shang, Z., Tian, J., Wang, Y., Zhang, T., Tang, Y.Y.: Spectral-spatial graph convolutional networks for semisupervised hyperspectral image classification. *IEEE Geosci. Remote Sensing Lett.* 16(2), 241–245 (2019)
21. Shi, L., Zhang, L., Yang, J., Zhang, L., Li, P.: Supervised graph embedding for polarimetric sar image classification. *IEEE Geoscience and Remote Sensing Letters* 10(2), 216–220 (2012)
22. Song, W., Li, S., Fang, L., Lu, T.: Hyperspectral image classification with deep feature fusion network. *IEEE Transactions on Geoscience and Remote Sensing* 56(6), 3173–3184 (2018)
23. Wang, H., Raiko, T., Lensu, L., Wang, T., Karhunen, J.: Semi-supervised domain adaptation for weakly labeled semantic video object segmentation. In: Asian conference on computer vision. pp. 163–179. Springer (2016)
24. Wang, H., Wang, T.: Primary object discovery and segmentation in videos via graph-based transductive inference. *Computer Vision and Image Understanding* 143, 159–172 (2016)
25. Wang, H., Wang, T., Chen, K., Kämäräinen, J.K.: Cross-granularity graph inference for semantic video object segmentation. In: IJCAI. pp. 4544–4550 (2017)
26. Wang, T., Wang, G., Tan, K.E., Tan, D.: Spectral pyramid graph attention network for hyperspectral image classification. *arXiv preprint arXiv:2001.07108* (2020)
27. Wang, T., Wang, H.: Graph transduction learning of object proposals for video object segmentation. In: Asian Conference on Computer Vision. pp. 553–568. Springer (2014)
28. Zhang, L., Zhang, Q., Du, B., Huang, X., Tang, Y.Y., Tao, D.: Simultaneous spectral-spatial feature selection and extraction for hyperspectral images. *IEEE Transactions on Cybernetics* 48(1), 16–28 (2016)
29. Zhong, Z., Fan, B., Duan, J., Wang, L., Ding, K., Xiang, S., Pan, C.: Discriminant tensor spectral–spatial feature extraction for hyperspectral image classification. *IEEE Geoscience and Remote Sensing Letters* 12(5), 1028–1032 (2014)
30. Zhou, F., Hang, R., Liu, Q., Yuan, X.: Hyperspectral image classification using spectral-spatial lstms. *Neurocomputing* 328, 39–47 (2019)